Characterization of the lasing properties of a 5%Yb doped Lu_2SiO_5 crystal along its three principal dielectric axes

Guido Toci,[1] Angela Pirri,[2,*] Alena Beitlerova,[3] Yasuhiro Shoji,[4] Akira Yoshikawa,[4,5] Jiri Hybler,[3] Martin Nikl,[3] and Matteo Vannini[1]

[1]*C.N.R.-National Research Council, Istituto Nazionale di Ottica Via Madonna del Piano 10, I-50019 Sesto Fiorentino (FI), Italy*

[2]*C.N.R.-National Research Council, Institute of Applied Physics "Nello Carrara" Via Madonna del Piano 10, I-50019 Sesto Fiorentino (FI), Italy*

[3]*Institute of Physics Academy of Sciences of the Czech Republic, Cukrovarnicka 10, Prague 162 53, Czech Republic*

[4]*Institute for Materials Research, Tohoku University, 2-1-1 Katahira, Aoba-ku, Sendai, 980-8577 Japan*

[5]*New Industry Creation Hatchery Center (NICHe), Tohoku University, 6-6-10 Aoba, Aramaki, Aoba-ku, Sendai, Miyagi 980-8579, Japan*

[*]*a.pirri@ifac.cnr.it*

Abstract: The laser performance of a 5% Yb doped Lu_2SiO_5 (Yb:LSO) has been investigated in quasi continuous-wave pumping regime along the three principal dielectric axes of the crystal, to obtain a complete characterization of its laser properties. The comparison among the obtained results for differently polarized lasers, in term of relative slope efficiency and absolute efficiency, allows the exploitability of different orientations of the material in order to be determined to obtain efficient laser sources. The laser slope efficiency and the energy conversion efficiency were similar for emission polarized along the three indicatrix axes, with noticeable maximum values of slope efficiency around 90% for polarization along the Y and Z axes. Tunable laser action has been obtained in the range 990 nm - 1084 nm, with sizeable differences in the shape of the tuning curve for polarization along the X, Y and Z axes. In particular, the tuning for polarization along the Z axis is relatively flat and uniform in the range 1023 nm - 1083 nm.

OCIS codes: (140.3615) Lasers, ytterbium; (140.5680) Rare earth and transition metal solid-state lasers; (140.3600) Lasers, tunable; (160.3380) Laser materials; (160.5690) Rare-earth-doped materials.

References and links

1. L. D. DeLoach, S. A. Payne, L. L. Chase, L. K. Smith, W. L. Kway, and W. F. Krupke, "Evaluation of absorption and emission properties of Yb3+ doped crystals for laser applications," IEEE J. Quantum Electron. **29**(4), 1179–1191 (1993).
2. F. Druon, S. Ricaud, D. N. Papadopoulos, A. Pellegrina, P. Camy, J. L. Doualan, R. Moncorgé, A. Courjaud, E. Mottay, and P. Georges, "On Yb:CaF_2 and Yb:SrF_2: review of spectroscopic and thermal properties and their impact on femtosecond and high power laser performance [Invited]," Opt. Mater. Express **1**(3), 489–502 (2011).
3. A. Pirri, G. Toci, and M. Vannini, "First laser oscillation and broad tunability of 1 at. % Yb-doped Sc_2O_3 and Lu_2O_3 ceramics," Opt. Lett. **36**(21), 4284–4286 (2011).
4. A. Pirri, M. Vannini, V. Babin, M. Nikl, and G. Toci, "CW and quasi-CW laser performance of 10 at.% Yb^{3+}:LuAG ceramic," Laser Phys. **23**(9), 095002 (2013).
5. L. Esposito, J. Hostaša, A. Piancastelli, G. Toci, D. Alderighi, M. Vannini, T. Epicier, A. Malchère, G. Alombert-Goget, and G. Boulon, "Multilayered YAG-Yb:YAG ceramics: manufacture and laser performance," J. Mater. Chem. C **2**(47), 10138–10148 (2014).
6. M. Jacquemet, C. Jacquemet, N. Janel, F. Druon, F. Balembois, P. Georges, J. Petit, B. Viana, D. Vivien, and B. Ferrand, "Efficient laser action of Yb:LSO and Yb:YSO oxyorthosilicates crystals under high-power diode-pumping," Appl. Phys. B **80**(2), 171–176 (2005).
7. F. Thibault, D. Pelenc, F. Druon, Y. Zaouter, M. Jacquemet, and P. Georges, "Efficient diode-pumped Yb^{3+}:Y_2SiO_5 and Yb^{3+}:Lu_2SiO_5 high-power femtosecond laser operation," Opt. Lett. **31**(10), 1555–1557 (2006).
8. N. Lin, W. Li, Y. Zhou, Y. Shi, M. Yan, K. Yang, J. Zhao, X. Yang, and H. Zeng, "High-power output of ytterbium-doped oxyorthosilicate lasers at 1018 nm," Laser Phys. Lett. **10**(1), 015103 (2013).

#231406 - $15.00 USD Received 26 Dec 2014; revised 4 Mar 2015; accepted 2 Apr 2015; published 12 May 2015

9. W. Tian, Z. Wang, J. Zhu, Z. Wei, L. Zheng, X. Xu, and J. Xu, "54 fs Kerr-lens mode-locking Yb:LSO laser," in Advanced Solid State Lasers, OSA Technical Digest (online) (Optical Society of America, 2014), paper AM5A.10.
10. A. Jolly, G. Bourdet, H. Coic, and J. Luce, "Gain versus tuning issues to Q-switch with Yb^{3+}:LSO and amplify broad-bandwidth pulses," Appl. Phys. B **97**(1), 85–94 (2009).
11. T. Gustafsson, M. Klintenberg, S. E. Derenzo, M. J. Weber, and J. O. Thomas, "Lu_2SiO_5 by single-crystal X-ray and neutron diffraction," Acta Crystallogr. C **57**(6), 668–669 (2001).
12. G. E. Jellison, E. D. Specht, L. A. Boatner, D. J. Singh, and C. L. Melcher, "Spectroscopic refractive indices of monoclinic single crystal and ceramic lutetium oxyorthosilicate from 200 to 850nm," J. Appl. Phys. **112**(6), 063524 (2012).
13. S. Campos, A. Denoyer, S. Jandl, B. Viana, D. Vivien, P. Loiseau, and B. Ferrand, "Spectroscopic studies of Yb^{3+}-doped rare earth orthosilicate crystals," J. Phys. Condens. Matter **16**(25), 4579–4590 (2004).
14. Z. Huang, G. Li, and Y. Qiu, "Power calculation of wavelength tunable Yb^{3+}:LSO laser," Opt. Express **18**(20), 20979–20987 (2010).
15. H. Cong, H. Zhang, J. Wang, W. Yu, J. Fan, X. Cheng, S. Sun, J. Zhang, Q. Lu, C. Jiang, and R. I. Boughton, "Structural and thermal properties of the monoclinic Lu_2SiO_5 single crystal: evaluation as a new laser matrix," J. Appl. Cryst. **42**(2), 284–294 (2009).
16. B. Boulanger, Y. Petit, P. Segonds, C. Félix, B. Ménaert, J. Zaccaro, and G. Aka, "Absorption and fluorescence anisotropies of monoclinic crystals: the case of Nd:YCOB," Opt. Express **16**(11), 7997–8002 (2008).
17. Y. Petit, S. Joly, P. Segonds, and B. Boulanger, "Recent advances in monoclinic crystal optics," Laser Photon. Rev. **7**(6), 920–937 (2013).
18. G. Boulon, "Why so deep research on Yb^{3+}-doped optical inorganic materials?" J. All. Comp. **451**(1-2), 1–11 (2008).
19. L. van Pieterson, M. Heeroma, E. de Heer, and A. Meijerink, "Charge transfer luminescence of Yb^{3+}," J. Lumin. **91**(3-4), 177–193 (2000).
20. A. Pirri, G. Toci, M. Nikl, V. Babin, and M. Vannini, "Experimental evidence of a nonlinear loss mechanism in highly doped Yb:LuAG crystal," Opt. Express **22**(4), 4038–4049 (2014).
21. C. W. Thiel and R. L. Cone, "Investigating material trends and lattice relaxation effects for understanding electron transfer phenomena in rare-earth-doped optical materials," J. Lumin. **131**(3), 386–395 (2011).
22. M. Nikl, A. Yoshikawa, and T. Fukuda, "Charge transfer luminescence in Yb^{3+}-containing compounds," Opt. Mater. **26**(4), 545–549 (2004).
23. P. Dorenbos, "Systematic behaviour in trivalent lanthanide charge transfer energies," J. Phys. Condens. Matter **15**(49), 8417–8434 (2003).
24. A. Pirri, D. Alderighi, G. Toci, M. Vannini, M. Nikl, and H. Sato, "Direct comparison of Yb^{3+}:CaF_2 and heavily doped Yb^{3+}:YLF as laser media at room temperature," Opt. Express **17**(20), 18312–18319 (2009).
25. J. A. Caird, S. A. Payne, P. R. Staver, A. J. Ramponi, and L. L. Chase, "Quantum electronic properties of the $Na_3Ga_2Li_3F_{12}$: Cr^{3+} laser," IEEE J. Quantum Electron. **24**(6), 1077–1099 (1988).
26. X. Y. Zhang, W. X. Li, K. W. Yang, H. Zhou, N. N. Lin, Z. Y. Pan, S. Y. Gu, Y. J. He, J. P. Huang, and H. P. Zeng, "High-power continuous-wave output of master oscillator power amplifier system at 1053 and 1083 nm," Laser Phys. **21**(10), 1789–1792 (2011).
27. K. Beil, B. Deppe, and C. Kränkel, "Yb:$CaGdAlO_4$ thin-disk laser with 70% slope efficiency and 90 nm wavelength tuning range," Opt. Lett. **38**(11), 1966–1968 (2013).
28. M. Siebold, S. Bock, U. Schramm, B. Xu, J. L. Doualan, P. Camy, and R. Moncorgé, "Yb:CaF_2 - a new old laser crystal," Appl. Phys. B **97**(2), 327–338 (2009).

1. Introduction

A huge number of studies on Yb doped solid state media have been published in the last decade. This widespread interest is motivated by the occurrence of several interesting features, and in particular: the small quantum defect (generally about 10%) that allows a low thermal load and high efficiency [1]; the broad absorption band that relaxes the requirement of tight wavelength control of the pumping wavelength, useful when pumping with semiconductor lasers; the generally broad emission spectrum of a large number of Yb-doped materials allows the realization of widely tunable sources and femtosecond oscillators [2]. Moreover there is a large availability of hosts that can be doped with Yb^{3+}, resulting in a broad variability in the spectroscopic, optical and thermomechanical properties, which results in the possibility to finely tune the choice of the material according to the specific application needs.

A further broadening in the palette of the available hosts has been achieved by the development of transparent ceramics, derived from isotropic single crystals [3,4]. Ceramics can offer unique advantages for specific laser applications with respect to their crystal counterparts, due to their higher flexibility in the fabrication and structuring of large high quality active media for high power applications [5].

#231406 - $15.00 USD Received 26 Dec 2014; revised 4 Mar 2015; accepted 2 Apr 2015; published 12 May 2015

In this framework Yb doped oxyorthosilicates and in particular Lu_2SiO_5 (LSO) as well as its isomorph Y_2SiO_5 have attracted some attention in the literature. These materials are optically biaxial crystals with three principal dielectric axes, and they combine a relatively high thermal conductivity, a very large tunability and broad absorption spectra [6]. LSO shows, with respect to YSO, a higher thermal conductivity when doped with Yb because the Yb molar mass is closer to Lutetium than to Yttrium [7].

Due to the anisotropy of the crystal structure in these materials the absorption and the emission spectra depend on the orientation of the polarization of the interacting radiation with respect to the principal dielectric axes. This feature offers a further degree of freedom in the design and development of laser devices. Until now, Yb:LSO has been studied in literature for CW, tunable laser emission [6, 8], for the generation of ultrashort pulses [7,9] and for the amplification of high-energy pulses [10]. Nonetheless, literature studies published so far focused their attention on only one polarization direction (typically along the X indicatrix axis, according to the classification described by Jacquemet *et al.* [6] and Jolly *et al.* [10]). In order to fill this gap we present in this work a complete characterization of the laser properties for a 5% Yb:LSO crystal. The laser emission properties (slope efficiency, tuning range) are characterized under laser diode pumping in uniform excitation conditions, with polarization along the three principal dielectric axes available with this crystal. To our knowledge this is the first analysis carried on the laser performances of the three available polarizations of this interesting Yb host.

2. Experimental set-up

2.1 Sample growth, orientation and spectroscopy

The Yb:LSO sample used in this work was grown by the Czochralski method using an iridium crucible with a diameter of 100 mm. The crucible was heated by induction at a frequency of 8 kHz. The growth atmosphere was Ar gas flow, and an undoped LSO single crystal was used as a seed. The pulling rate was 1 mm/hour and the rotation rate was 10 rpm. The Yb doping level was 5 at.%. 5N purity Lu_2O_3 and Yb_2O_3 powders and 4N purity SiO_2 powders were used as raw materials.

LSO has a monoclinic crystal structure, the space group is *C2/c,* and point group C_{2h} [11, 12]. The space group comprises the twofold rotation axis along the *b* direction of the lattice cell, and glide plane perpendicular to *b*, with translation component parallel to *c*. The axes *a* and *c* are perpendicular to *b*, and they form an angle of about 122°.

The high symmetry axis along *b* is also one of the principal axes of the dielectric tensor. In the orthogonal reference frame made by the lattice axes *a*, *b* and by the reciprocal lattice axis *c** the dielectric tensor is not diagonal. As recently shown by Jellison *et al*. [12], in the visible and in the near infrared the real part of the dielectric tensor is symmetric; the only non-zero off-diagonal term ε_{12} is small and nearly constant with respect to the wavelength. Therefore the real part of the dielectric tensor can be diagonalized by rotating the reference frame by a small angle around *b.* This new reference frame is therefore the principal dielectric reference frame, and its axes D_1, D_2 and *b* are coincident with the indicatrix axes.

For the sample used in this experiment, we first determined the orientation of the *a*, *b*, and *c* axes by means of X-ray diffraction (back-reflection Laue method). A plane parallel slab was then cut with the facets perpendicular to the *b* axis. On this slab, we then further verified the orientation of the two indicatrix axes with respect to *a* and *c* by means of transmission measurements with crossed polarizers. Then the slab was cut in its final parallelepiped shape with the two remaining edges parallel to the indicatrix axes. The resulting orientation of the sample is depicted in Fig. 1. The dielectric axis D_1 is the one closer to *a*.

#231406 - $15.00 USD Received 26 Dec 2014; revised 4 Mar 2015; accepted 2 Apr 2015; published 12 May 2015

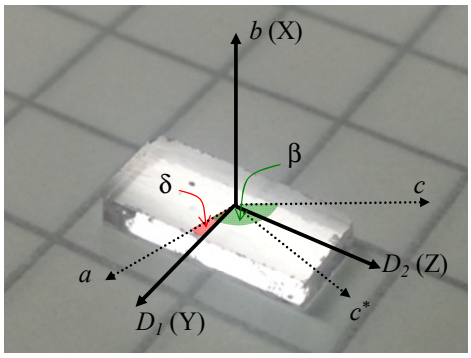

Fig. 1. Orientation of the sample with respect to the (direct) lattice axes *a,b,c,* and to the reciprocal lattice axis *c** and with respect to the dielectric principal axes D_1 and D_2 (indicatrix axes). D_1, D_2 and *b* are mutually orthogonal. The angle δ is about 16°, β = 122°.

The dimensions of the sample are 3.65 mm along D_1, 7 mm along D_2 and 1.29 mm along *b*. From the results provided by Jellison *et al.* [12] it turns out that between 200 nm and 850 nm for the refractive index it is $n(b)<n(D_1)<n(D_2)$. Using the standard convention for the nomenclature of the axes of biaxial crystals ($n_X<n_Y<n_Z$) the axes association is therefore $b \rightarrow X$, $D_1 \rightarrow Y$, $D_2 \rightarrow Z$. It must be noticed that according to [12] the difference between n_X and n_Y is very small, so from the measurement of the refractive indices the X and Y axes can be easily exchanged. In the following part of the paper we then will use the labeling *b*, D_1, D_2 because it is more closely related to the lattice axes than to the determination of the refractive indices. Anyway, the connection with the standard nomenclature has been established above.

We note that for the angle δ between D_1 and *a* we found a slightly larger value (16°) than the value estimated in Ref. [12] (about 10°). This discrepancy can depend from several reasons: firstly, the exact value of δ depends from the off-diagonal term ε_{12}, which is determined in [12] with a relatively large error due to its small value. Accounting for the random measurements errors in [12], δ can range from 3.1° to 13.8°. Moreover, both our measurements and those reported in [12] are affected by a systematic uncertainty in the orientation of the sample, of the order of 1°, and this could also affect the determination of δ. Finally the data of Ref. [12] are measured on an undoped LSO sample. Yb doping could slightly modify the values of the dielectric tensor elements.

In LSO, Yb substitutes Lu, and it can occupy two different lattice sites [13], with different energy levels positioning [14]. The overall absorption and emission spectra result therefore from the superimposition of the spectra of the two different sites. The upper laser level lifetime is 0.95 ms [6]. The thermal conductivity is anisotropic, and the values of the principal components of the thermal conductivity tensor are 2.26, 3.14 and 3.67 W m^{-1} K^{-1} in undoped LSO [15].

It must be noticed here that the direction of the axes of the indicatrix correspond to the principal dielectric reference frame. As it has been pointed out by Petit *et al.* [16,17] for monoclinic crystals this frame does not necessarily diagonalize the imaginary part of the dielectric tensor (which describes the absorption and the fluorescence). The reference frames that diagonalize the imaginary part of the dielectric tensor for absorption or emission are in principle different both from the principal dielectric reference frame and from each other.

To our knowledge, the characterization of principal reference frames for absorption and fluorescence was never reported in literature for Yb:LSO. This requires specific measurement techniques of the direction and polarization properties of the fluorescence spectra that were not carried out for this paper, and will be the subject of possible further activities.

Absorption cross section spectra of the Yb dopant are shown in Fig. 2(a), measured with a spectral resolution of 3 nm. The absorption peaks at about 900 nm, 920-925 nm and 975-980 nm are due to the transitions from the lowest level of the lower $^2F_{7/2}$ multiplet to three levels of the upper $^2F_{5/2}$ multiplet [18]. Peak broadening and/or slight shifts and other subpeaks in

#231406 - $15.00 USD Received 26 Dec 2014; revised 4 Mar 2015; accepted 2 Apr 2015; published 12 May 2015

900-1020 nm spectral region can also be due to the fact that there are two Lu sites of different symmetry and Yb^{3+} energy level positioning as mentioned above.

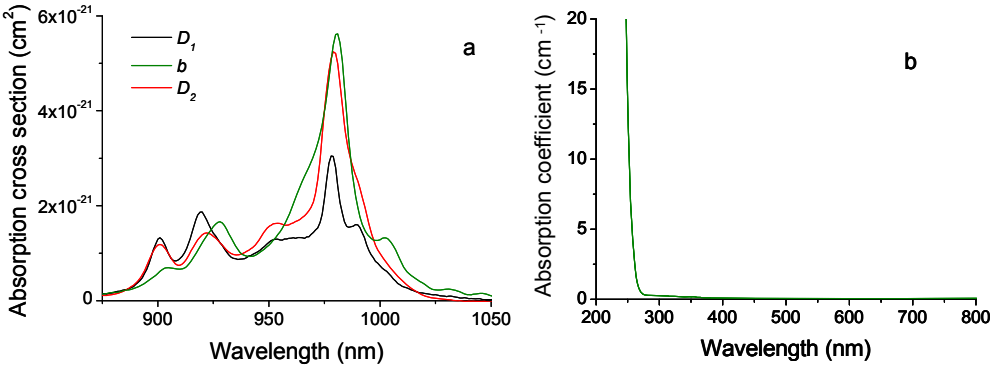

Fig. 2. Absorption cross section of the 5% Yb doped LSO. (a): absorption cross section of the transition $^2F_{7/2} \rightarrow {}^2F_{5/2}$ of the Yb^{3+} ion, for polarization parallel to the three principal dielectric axes. (b): near IR to UV absorption spectrum of the sample for polarization along the D_1 dielectric axis.

It is useful to compare these spectra with those previously reported in literature, in order to establish a connection with previous results. The absorption cross section spectra that we measured are similar to those reported in [10], with the correspondence (D_1, b, D_2 this work $\rightarrow$ X,Y,Z in [10]). Indeed the spectrum for D_1 polarization can be discriminated from the other two because its peak near 970 nm is relatively weak in comparison with the plateau a shorter wavelengths, with respect to the spectra for b and D_2 polarization; the spectrum polarized along b features a peak at about 1005 nm which is not present on the D_2 polarization. By comparing these features with the spectra published in [10] it appears that with respect to our results the attributions of the axes X and Y in [10] have to be exchanged. A further difference is that we have measured a somewhat lower peak absorption cross section for all the three polarization axes, and in particular for the b (Y in [10]) polarization, which is about 30% lower.

Figure 2(b) show the absorption spectrum on a broader spectral range, from UV to near infrared. Sharp increase of absorbance below 270 nm is due to charge transfer (CT) absorption transition from oxygen ligands forming the top of valence band towards Yb^{3+}[19]. Comparing analogous spectra for the Yb-doped LuAG [20] and LSO hosts, the shift toward higher energy by about 10 nm that appears in the former case can be due to slight variation of the absolute position of oxygen levels at the top of valence band induced by site symmetry and crystal field strength, and by small shifts in the positioning the ground state of Yb^{2+} which determines quantitatively the onset of this CT transition [21–23].

2.2 Laser experimental set-up

The sample has been characterized in a V-shaped laser cavity as shown in Fig. 3. The crystal is optically pumped with a diode laser with emission wavelength of 969 nm coupled to a fiber with a 100 μm core diameter and a NA of 0.12. The pump beam is focused on the sample by means of a pair of achromatic doublets (focal length 60 mm, clear aperture 30 mm). The doublets assembly was set at about 60 mm from the fiber end and from the sample; this arrangement gives a unit magnification ratio resulting in a waist radius of 70 μm at $1/e^2$ and a Rayleigh range of about 0.58 mm in air (corresponding to about 1.05 mm in the crystal). The waist radius on the crystal is slightly larger than the fiber radius because of the residual spherical aberration of the lens pair. The pump beam characterization was carried out with a CCD camera and a beam analysis software. The pump beam is injected into the cavity through the dichroic flat end mirror M1, having a high transmission for wavelength shorter

#231406 - $15.00 USD Received 26 Dec 2014; revised 4 Mar 2015; accepted 2 Apr 2015; published 12 May 2015

than 980 nm and high reflectivity for wavelength higher than 990 nm. The pump beam is unpolarized.

The cavity is folded by a small angle by a dichroic mirror FM (high reflectivity for $\lambda > 990$ nm, high transmission for $\lambda < 980$ nm) with a radius of curvature of 100 mm. The residual pump beam is transmitted by this mirror. The non-tunable cavity is completed with a fused silica plate set at the Brewster angle for the polarization selection and with a flat output coupler mirror for which various transmissions (T_{OC}) between 1.7% and 18.4% have been used. The tunable cavity (see the inset in Fig. 3) is realized by removing the Brewster plate and inserting a prism (made of SF10 glass) set at the minimum deviation configuration, and a flat output coupler. The prism apex angle is 60° and it can be set with both faces close to the Brewster angle, so that the prism itself acts as a horizontal polarization selector. Wavelength selectivity is further enhanced by the slit set near to the prism apex.

The crystal does not have antireflection coating, and it was carefully oriented so as to reinject the Fresnel reflection at the surfaces back on the cavity axis, in order to minimize reflection losses. The crystal was placed as near as possible (less than 1 mm) to M1.

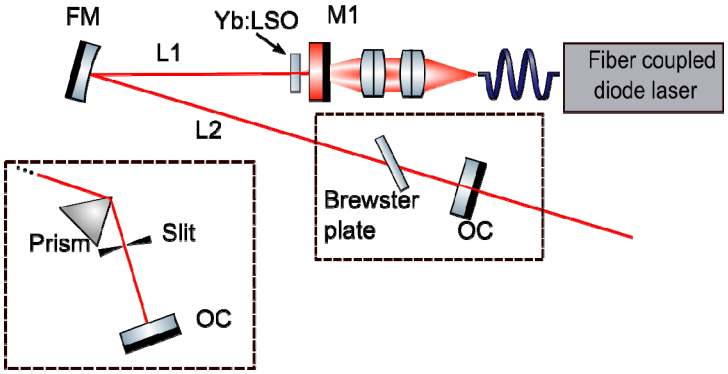

Fig. 3. Set up of non tunable and tunable laser cavities. See the text for detailed description. L1 = 59 mm, L2 = 200 mm.

The crystal was soldered with Indium on a copper heat sink on its D_1-D_2 face. For the investigation of the lasing properties with polarization along the D_1 and D_2 axes the beam propagation direction was set along the *b* axis and the crystal was thus end-cooled with respect to the laser and pump beam propagation direction. In the following this will be referred to as A configuration. For the analysis of the laser behavior with polarizations along the D_2 and *b* axes the beam propagation direction was along the D_1 axis and the crystal was side-cooled with respect to the beam propagation: this arrangement will be referred to as B configuration. Two different heat sinks were used as exemplified in Fig. 4. The propagation along the D_2 axis does not allow an efficient pumping because the crystal is much longer than the depth of focus of the pump beam. The orientation of the beam polarization (as determined by the position of the Brewster plate or of the prism) with respect to the crystal axes is obtained by rotating the sample and the heat sink around the beam propagation axis.

#231406 - $15.00 USD Received 26 Dec 2014; revised 4 Mar 2015; accepted 2 Apr 2015; published 12 May 2015

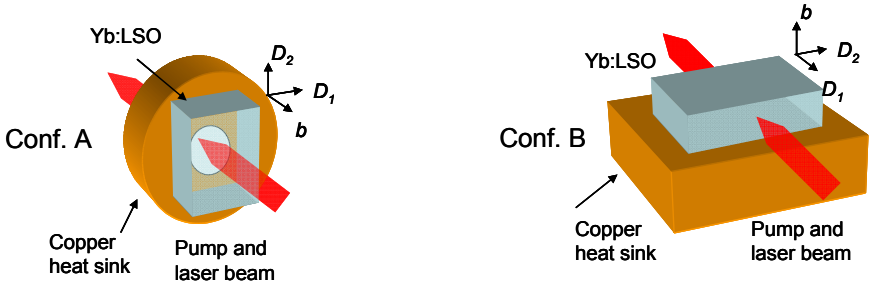

Fig. 4. Arrangement of the crystal and of the copper heat sink for the measurement with the different axes orientations, *i.e.* configurations A and B as defined in the text. The orientations of the principal dielectric axes in the two configurations are also shown.

To reduce the impact of thermal effects, the pump laser diode is operated with rectangular pulses at 10 Hz of repetition frequency and 20% of duty factor. For both configurations the maximum laser power incident on the sample was 19.1 W (peak power, *i.e.* during the pump on period). In order to compare the performances of the samples, the geometry of the set-up has been kept constant through all the measurements. Lasing emission spectra were analyzed with a spectrometer equipped with an optical multichannel analyzer (EG&G OMA 2000), with an overall wavelength resolution of 0.2 nm.

3. Measurements of laser performances

3.1 Slope efficiencies and threshold measurements

The laser performance of the sample was tested with the two alignment described in Fig. 4. Several output couplers were used with different values of transmission, ranging from 1.7% to 18.4%.

In order to properly evaluate the absorbed pump power we monitored the power of the residual pump beam transmitted by the sample with an auxiliary power monitor placed behind the folding mirror FM (see Fig. 3). The correction for the Fresnel reflection at the crystal interfaces was also properly applied. As it was pointed out in previous papers [24] the actual sample absorption in lasing conditions (that is under high pump and laser power density) is usually different from the unsaturated absorption (*i.e.* with low incident power density, that can be calculated from the spectroscopic data), as it is influenced by two counteracting effects: on one hand the absorption saturation caused by the high pump power density (which reduces the power deposition into the sample), and on the other hand the rapid deexcitation of the lasing ions from the upper laser level to the ground level, which restores the population on the ground level and thus the absorption of the pump beam. The balance of these two effects depends both on the pump power density and on the laser intracavity power density, and thus on the transmission of the output coupler.

Figures 5 and 6 show the obtained output power as a function of absorbed pump power. Figure 5 refers to the configuration A shown in Fig. 4, that is with propagation along the *b* crystal axis and polarization along the D_1 and D_2 axes. In this orientation the unsaturated absorption of the crystal was about 16%. In this configuration, if we take out the Brewster plate polarizer from the cavity, the laser action occurs spontaneously with polarization along the D_1 direction, whereas lasing with polarization along the D_2 direction can be obtained only by forcing it with the polarizer. Anyway, the measurements reported in Fig. 4 were acquired with the intracavity polarizer for both polarizations to ensure uniform test conditions.

#231406 - $15.00 USD Received 26 Dec 2014; revised 4 Mar 2015; accepted 2 Apr 2015; published 12 May 2015

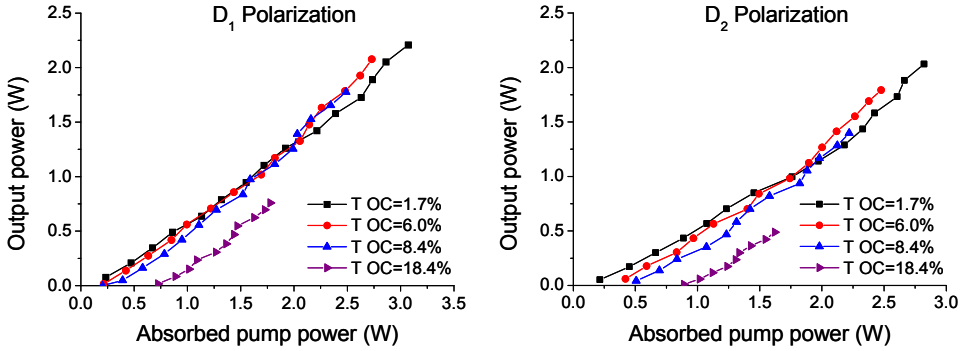

Fig. 5. Quasi-CW output power as function of absorbed pump power for the lasing configuration A (see Fig. 4) for various values of T_{OC}.

The lasing wavelength for the D_1 polarization is 1057 nm for T_{OC} = 1.7% and it slightly drifts to 1056 nm for increasing values of T_{OC}. For lasing along the D_2 polarization the behavior is more complex: for T_{OC} = 1.7% the lasing wavelength is 1056.2 nm. For increasing values of T_{OC} the laser emission occurs on two lines, at 1056 and 1040 nm. Finally, for the highest value of T_{OC} the lasing wavelength further shifts to 1033.8 nm.

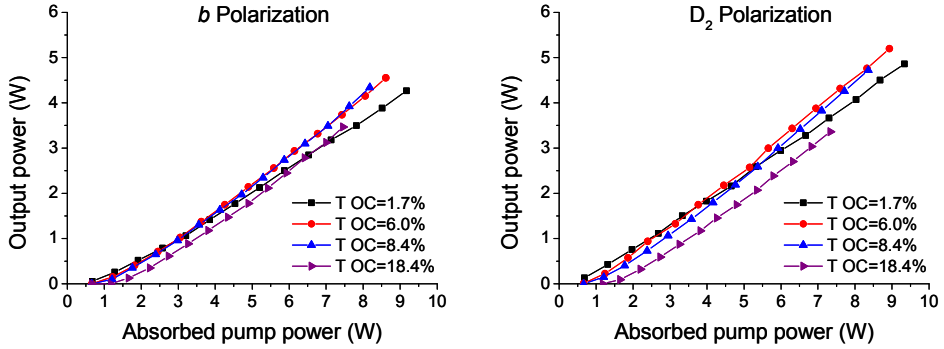

Fig. 6. Quasi-CW output power as function of absorbed pump power for the lasing configuration B (see Fig. 4), for various values of T_{OC}.

Figure 6 refers to the configuration B, *i. e.* with propagation along the D_1 axis and polarization along the *b* and D_2 axes. Without the intracavity polarizer, lasing occurs with polarization along the D_2 axis. Again, the measurements of Fig. 6 were acquired with the intracavity polarizer for both polarizations. In this case the unsaturated absorption was about 49%, mainly due to the longer absorption length of the sample.

Regarding the lasing wavelength, for the D_2 polarization it is 1057.4 nm for T_{OC} = 1.7% and it slightly drifts to 1056 nm for increasing values of T_{OC}. For *b* polarization, lasing occurs at 1057.4 nm with T_{OC} = 1.7%; with T_{OC} = 6.0% and 8.4% it moves at 1034 nm, and to 1031.7 nm with T_{OC} = 18.3%. In all the mentioned configurations, the output of the laser was found linearly polarized (coherently with the orientation of the intracavity polarizer) with a polarization contrast better than 500:1, measured with a calcite Glan prism.

3.2 Tuning measurements

As exposed above, tunable lasing was obtained by inserting a prism into the cavity. Tuning is obtained by adjusting the position of the prism near to the minimum deviation angle. The tuning curves obtained for the laser output, for the various crystal orientations and laser output polarization are shown in Figs. 7 and 8 respectively. The output coupler used in this

#231406 - $15.00 USD Received 26 Dec 2014; revised 4 Mar 2015; accepted 2 Apr 2015; published 12 May 2015

case is the one with T_{OC} = 1.7%. The figures also report the curves for the power conversion efficiency *i. e.* the ratio between the output power and the absorbed pump power, for each wavelength.

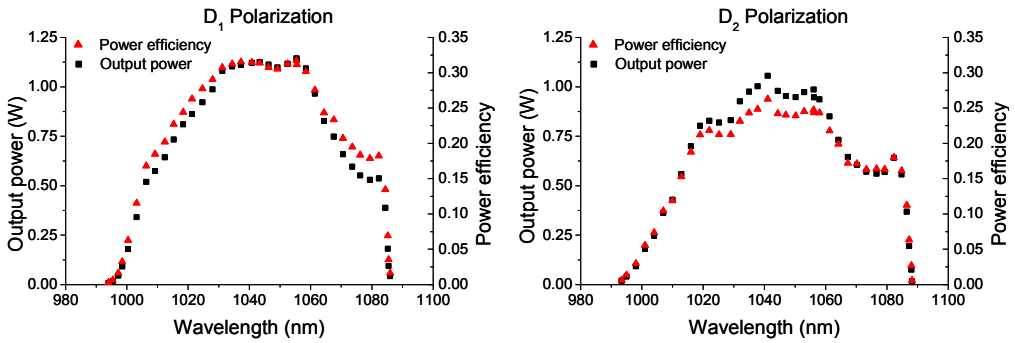

Fig. 7. Tuning for A configuration (propagation along the *b* crystal axis and polarization along the D_1 and D_2 axes, see Figs. 1 and 4), in quasi-CW pumping mode.

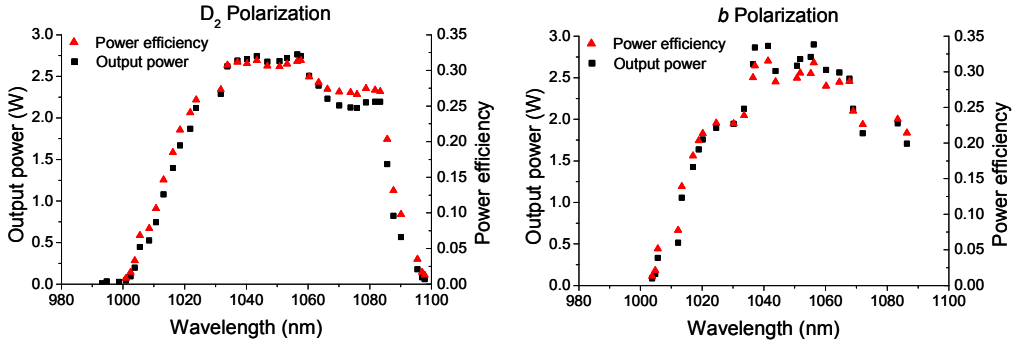

Fig. 8. Tuning for B configuration (propagation along D_1 axis, polarization along D_2 and *b* axes, see Figs. 1 and 4) in quasi-CW pumping mode.

For the A configuration (that is, propagation along the *b* axis, polarization along the D_1 and D_2 axes) it was possible to obtain a smooth and continuous tuning in the range between about 990 nm and 1090 nm, with a peak output power exceeding 1 W.

For the B configuration (propagation along D_1, polarization along D_2 and *b*) the output power was higher (exceeding 2.5 W), because as exposed before with this orientation the crystal absorbs a larger amount of the incident pump power. The tuning range for polarization along the D_2 axis was even slightly broader than that observed in the A configuration (stretching almost to 1100 nm), but with a wavelength jump between 1025 nm and 1030 nm: when the prism position is adjusted to move the wavelength from 1025 nm to longer wavelengths, at first the emission of the laser splits between two lines at 1025 nm and 1030 nm; a further rotation of the prism increases the relative power at 1030 nm until the emission at 1025 nm is extinguished; from this point the continuous tuning toward wavelengths longer than 1030 nm is resumed. For the emission polarized along the *b* axis, the peak output power is even higher (up to 3 W) as well as the power efficiency (exceeding 30%), but with a narrower tuning range (from 1004 nm to 1086 nm). Moreover, we observed wavelength jumps (as described above) between 1072 nm and 1083 nm, and between 1050.8 nm and 1043 nm.

#231406 - $15.00 USD Received 26 Dec 2014; revised 4 Mar 2015; accepted 2 Apr 2015; published 12 May 2015

4. Discussion

The measurements described above allow obtaining a clear comparison among the laser performances that can be obtained with the different orientations of Yb:LSO. It must be noticed that the conditions in the two configurations are not completely equivalent: in particular the A configuration, with its short absorption length and small overall absorption, features a more uniform pump power density deposition and probably a better geometrical matching between the pump beam and the lasing modes, with respect to the B configuration which has a stronger absorption and a longer absorption length (and then a more noticeable defocusing of the pump beam along the propagation). The cooling conditions are also not exactly equivalent, as exposed above.

The use of a different pumping and cooling geometry for the two orientations was not deliberate, but it was forced by the small size of the available sample. In order to set a similar geometry it would be necessary to cut from the sample a slice with a thickness of 1.3 mm across the D_1 direction, but the resulting piece would have a too small contact surface with the heat sink and would probably not withstand to the thermomechanical stress associated with the pumping process.

On the other hand, the laser action along the D_2 polarization can be explored both in the A and in the B configuration, and this information can be used to intercompare the results for the X and Y polarization, independently from the geometrical differences.

Table 1 reports the slope and power conversion efficiencies obtained for the A configuration (propagation along *b*, polarization along D_1 and D_2 polarization). It can be seen that both in D_1 and in D_2 polarization the sample reaches very high slope efficiencies η_{SL}, as high as 91.6% with respect to the absorbed pump power. To our knowledge, this is one of the highest values of slope ever reported for Yb doped materials. Overall, the D_1 polarization has a slightly better performance than the D_2 polarization, as for each value of T_{OC} it features a slightly higher value of the slope efficiency, of the energy conversion efficiency η_{EFF} and a lower value of the threshold power for the laser action.

Table 1. - Slope efficiency η_{SL}, power conversion efficiency η_{EFF} and threshold power P_{th} for propagation along *b*, polarization along D_1 and D_2 (A configuration of Fig. 4), and various values of the transmission of the output coupler T_{OC}.

T_{OC}	Pol.	η_{SL}%	η_{EFF}%	P_{th} (W)	Pol.	η_{SL}%	η_{EFF}%	P_{th} (W)
1.7%	D_1	79.6	71.8	0.12	D_2	82.7	72.0	0.13
6.0%	D_1	91.6	76.0	0.19	D_2	91.0	72.3	0.31
8.4%	D_1	90.6	71.4	0.32	D_2	88.4	62.9	0.45
18.3%	D_1	78.9	42.7	0.70	D_2	70.6	31.3	0.89

These high values of slope efficiency are due to the very high quality of the material (featuring very low parasitic losses) but also to a very favorable geometric condition, as explained above, that is a rather short crystal length and a rather low absorption: both elements contribute to have a very uniform pump intensity distribution along the sample length.

Table 2. - Slope efficiency η_{SL}, power conversion efficiency η_{EFF} and threshold power P_{th} for propagation along D_1, polarization along *b* and D_2 (B configuration of Fig. 4), and various values of the transmission of the output coupler T_{OC}.

T_{OC}	Pol.	η_{SL}%	η_{EFF}%	P_{th} (W)	Pol.	η_{SL}%	η_{EFF}%	P_{th} (W)
1.7%	*b*	53.3	46.5	0.56	D_2	57.2	52.0	0.42
6.0%	*b*	63.1	52.8	0.91	D_2	67.1	58.1	0.69
8.4%	*b*	64.6	53.1	1.05	D_2	68.2	56.5	0.93
18.4%	*b*	60.6	46.5	1.41	D_2	60.4	45.8	1.47

Table 2 reports the values of slope efficiency, energy efficiency and lasing threshold obtained with the B configuration (propagation along D_1X, polarization along *b* and D_2). It can be seen that for this configuration the D_2 polarization has overall a slightly better performance than the *b* polarization, with slightly higher values of slope efficiency and

#231406 - $15.00 USD Received 26 Dec 2014; revised 4 Mar 2015; accepted 2 Apr 2015; published 12 May 2015

energy conversion efficiency, and lower values of threshold pump power. The only exception is with the OC having transmission of 18.4% where the *b* polarization gave slightly higher efficiencies and a slightly lower threshold. Fairly high values of slope efficiency, as high as 68%, were also obtained in this configuration.

The residual impact of the geometric conditions (mainly, the pump defocusing along the sample length) can be estimated by comparing the performance obtained for D_2 polarization with propagation along the *b* axis (Table 1), where the absorption length is 1.29 mm, and along the D_1 axis (Table 2, absorption length 3.65 mm). The poorer matching between the pump beam and the laser beam reduces the best slope efficiency from 91% to 68.2%, and increases the minimum threshold from 0.13 W to 0.42 W.

In order to obtain a clearer insight regarding the impact of the different geometrical conditions of the configurations A and B on the laser performances, we carried out a Caird analysis on the slope efficiencies obtained with the different output couplers. The values of slope efficiency η_{SL} of Tables 1 and 2 were fitted with the following equation

$$\eta_{SL} = \eta_P \frac{\lambda_P}{\lambda_L} \frac{T_{OC}}{T_{OC} + L} \tag{1}$$

where T_{OC} is the output coupler transmission, L are the round-trip parasitic losses and η_P is the pump coupling efficiency [25], λ_P and λ_L are the pump and the lasing wavelength respectively. L and η_P were used as fitting parameters. For the A configuration, polarization along D_1 we obtained $\eta_P = 0.96$ and L = 0.0014, whereas for the B configuration, D_2 polarization we obtained $\eta_P = 0.74$ and L = 0.0021. This result confirms that the lower overall efficiency of the B configuration was mainly due to a poorer pump matching, whereas the round trip losses (which include not only the internal losses in the crystal, but also the residual losses on the mirrors and the residual Fresnel reflections at the crystal surfaces) were very low and almost comparable in both configurations. We did not extend this analysis to the other two cases of Table 1 and 2 (configuration A, D_2 polarization and configuration B, *b* polarization) because in these cases a shift of the lasing wavelength was observed when changing T_{OC}, and this could make Eq. (1) not applicable.

From these results it can be also inferred that in the same geometrical conditions the *b* polarization would perform less well than the D_1 polarization.

In order to compare the tuning performance between the different orientations it is better to refer to the power conversion efficiency, rather than to the output power, because as we have explained above the crystal absorption changes significantly for the different orientations here considered, and so it does the laser output power. The power conversion efficiency provides a comparison that is less affected by the overall absorption.

Regarding the tuning ranges, in the A configuration (propagation along *b*, polarization along D_1 and D_2 polarization, see Fig. 7), a very broad tuning range, with a very similar extension, was obtained both for the D_1 (from 994 nm to 1086 nm) and for the D_2 polarization (from 993 nm to 1088 nm). The shape of the tuning curve shows some differences:, the tuning curve for the D_2 polarization is more flat than the D_1 tuning curve and exhibits a more uniform behavior in particular in the range from 1023 nm to 1083 nm. The peak power conversion efficiency is similar for the two polarizations, with a slight advantage for the D_1 polarization, which reflects the slightly higher values of slope efficiency found for the non-tunable operation.

Considering the B configuration (propagation along D_1, polarization along D_2 and b, see Fig. 8), we see that for D_2 polarization the overall power conversion efficiency is similar to that measured in the A configuration, but the tuning range now is more extended on the side of longer wavelengths, reaching up to 1098 nm. This is probably due to the fact that with this orientation the sample absorbs a larger portion of the pump power, allowing reaching lasing threshold more easily in the red end of the emission band, where the emission cross section is smaller. On the other hand, the wavelength span for shorter wavelength is slightly reduced,

#231406 - $15.00 USD Received 26 Dec 2014; revised 4 Mar 2015; accepted 2 Apr 2015; published 12 May 2015

most probably due to the larger impact of the ground level absorption in the sample regions subjected to a low pump power density.

Regarding the *b* polarization, its accessible tuning range is narrower than that recorded for the D_2 polarization, spanning from 1003 nm to 1086 nm. Moreover, we have found it rather difficult to have a smooth tuning along this wavelength range, with two wavelength jumps between 1072 and 1083 nm, and between 1050.8 nm and 1043 nm. Therefore, *b* polarization seems to be less favorable for tunable or broadband operation, even though the peak power conversion efficiency is well comparable with the D_1 and D_2 polarization.

The tuning ranges here reported are among the broadest obtained with Yb doped materials. To our knowledge, the broadest tuning ranges with Yb-doped materials were obtained so far with orthosilicates as LSO, YSO and LYSO, with Yb:$CaGdAlO_4$, and with fluorites. In particular, Zhang *et al*. have obtained a tuning range from about 995 nm to 1100 nm with the Yb-doped orthosilicates LSO, YSO and LYSO [26]. Beil *et al*. recently reported a tuning range extending from 1000 nm to 1090 nm and a CW output power of several watts, with a thin disk laser based on Yb:$CaGdAlO_4$ (Yb:CALGO) [27]. Regarding Yb-doped fluorites such as CaF_2 and SrF_2, it was demonstrated a tuning range 1000 nm - 1072 nm and 1005 nm - 1077 nm respectively [28].

5. Conclusions

In this work we have extensively characterized the laser performance of the Yb:LSO crystal along all its three principal dielectric axes. This characterization fills a gap in the literature, where the Yb:LSO is usually employed in laser devices for polarization emission along its X principal dielectric axis.

We have found that in terms of overall laser efficiency the three dielectric axes have rather similar performance, even though the X polarization has a slightly higher efficiency than the Z polarization and this latter in turn performs slightly better than the Y polarization. Anyway the differences are not dramatic, and therefore in the design of a specific device or application the choice of the crystal orientation and of the lasing polarization other than the X could be driven by other factors than the overall efficiency (e.g. anisotropy of the thermal conductivity, ease of growth along a specific direction, and so on), with small or no drawbacks in terms of the laser efficiency itself.

We were able to reach very high levels of the laser slope efficiency and the power conversion efficiency, as high as 91% for the slope efficiency for polarization along the D_1 dielectric axis in the most favorable conditions. It must be underlined that this is one of the highest slope efficiencies reported in literature not only for Yb:LSO, but in general for all Yb doped materials.

Regarding the tuning range, our measurements have shown that both the D_1 and D_2 orientation features a broad tuning range, which spans more than 90 nm. The tuning curve along the two orientations shows some interesting differences, in particular the tuning for polarization along the D_2 axis is significantly flat and uniform in the range from 1023 nm to 1083 nm (more than the tuning for polarization along the D_1 axis in the same range). This feature could be advantageously exploited in specific applications, such as for the development of ultrashort pulse amplifiers, because would result in a lesser distortion of the pulse spectrum during the amplification with respect to other amplifying media.

Acknowledgments

This activity has been supported by the CNR-AVCR Joint Project 2013-2015 “Influence of composition and defects on the properties of transparent ceramics and crystals for laser and scintillator applications.”

#231406 - $15.00 USD Received 26 Dec 2014; revised 4 Mar 2015; accepted 2 Apr 2015; published 12 May 2015